In Operando Modulation of Rectification in Molecular Tunneling Junctions Comprising Reconfigurable Molecular Self-Assemblies

Qiu, Xinkai; Rousseva, Sylvia; Ye, Gang; Hummelen, Jan C.; Chiechi, Ryan C.

Published in:
Advanced materials

DOI:
10.1002/adma.202006109

Publication date:
2021

ADVANCED MATERIALS
www.advmat.de

In Operando Modulation of Rectification in Molecular Tunneling Junctions Comprising Reconfigurable Molecular Self-Assemblies

*Xinkai Qiu, Sylvia Rousseva, Gang Ye, Jan C. Hummelen, and Ryan C. Chiechi**

The reconfiguration of molecular tunneling junctions during operation via the self-assembly of bilayers of glycol ethers is described. Well-established functional groups are used to modulate the magnitude and direction of rectification in assembled tunneling junctions by exposing them to solutions containing different glycol ethers. Variable-temperature measurements confirm that rectification occurs by the expected bias-dependent tunneling–hopping mechanism for these functional groups and that glycol ethers, besides being an unusually efficient tunneling medium, behave similarly to alkanes. Memory bits are fabricated from crossbar junctions prepared by injecting eutectic Ga–In (EGaIn) into microfluidic channels. The states of two 8-bit registers were set by trains of droplets such that they are able to perform logical AND operations on bit strings encoded into chemical packets that alter the composition of the crossbar junctions through self-assembly to effect memristor-like properties. This proof-of-concept work demonstrates the potential for fieldable devices based on molecular tunneling junctions comprising self-assembled monolayers and bilayers.

Ever-evolving, modern computing hardware, from processors to memory storage, relies on electronic components of extremely small size and high energy efficiency.[1] Molecular tunneling junctions, in which the charge transport properties of molecules are exploited in devices, have considerable potential in this context because subtle changes at the atomic scale can translate into unique and useful effects at the device level.[2,3] By exploiting the chemical nature of molecular electronics, these effects are exemplified in photoisomerization,[4–8], protonation,[9,10] electrostatic gating,[11,12] reduction–oxidation,[13] etc., giving rise to molecular resistors and molecular diodes in both single-molecule junctions and large-area junctions comprising self-assembled monolayers (SAMs). The majority of studies on effects that rely on external inputs, such as conductance switching, are observed ex situ, i.e., new junctions are formed and characterized instead of molecules being switched in-place, be they single-molecule break-junctions in which molecules are repeatedly trapped and released[14] or large-area junctions formed by raising and lowering a tip on top of a SAM.[9] Static, single-molecule junctions that exhibit in situ conductance switching often suffer from instability at room temperature and low yield of working junctions;[8,15] device-like, large-area junctions comprising SAMs, on the contrary, have demonstrated reproducible conductance switching at ambient conditions.[3,16] Technological applications of molecular electronics, particularly in computation, will require in situ and in operando (during operation) switching, which can be accomplished by exploiting reconfigurable molecular self-assembly and the properties of charge transport at the molecular scale to affect the electrical properties of a molecular-electronic device while in operation.[17]

Self-assembled bilayers (SABs) of triethylene-glycol-functionalized fulleropyrrolidines (**PTEG-1**) are a drop-in replacement for conventional thiol-based SAMs as an air-stable platform for molecular (tunneling) junctions.[18] The interdigitation of glycol ethers (GEs) drives the formation of a bilayer with tunable charge transport properties via reversible exchange with arbitrary GEs. SABs of GE-functionalized fullerenes exhibit asymmetric charge transport, but this phenomenon is absent in monolayers of **PTEG-1**, for which the dominant mechanism of charge transport is non-resonant tunneling.[18] The origins of asymmetric charge transport in molecular junctions are often ascribed to: 1) the formation of a Schottky diode,[19] 2) Stark shifts in molecular orbitals,[9,20,21] 3) the alignment between the molecular dipole moment and the external electric field[22,23] or 4) bias-dependent, thermally activated processes mediated by molecular frontier orbitals combined with non-resonance tunneling, which we will refer to as the tunneling–hopping mechanism.[24–26] SAMs of alkanethiols bearing fullerene headgroups exhibit asymmetric charge transport that is ascribed to a thermally activated process (the hopping part of tunneling-hopping) mediated by the lowest unoccupied π-state (LUPS) of the fullerene cage; the LUPS is pushed out of resonance at

X. Qiu, S. Rousseva, Dr. G. Ye, Prof. J. C. Hummelen, Prof. R. C. Chiechi
Stratingh Institute for Chemistry
University of Groningen
Nijenborgh 4, 9747 AG Groningen, Netherlands
E-mail: r.c.chiechi@rug.nl

X. Qiu, S. Rousseva, Dr. G. Ye, Prof. J. C. Hummelen, Prof. R. C. Chiechi
Zernike Institute for Advanced Materials
University of Groningen
Nijenborgh 4, 9747 AG Groningen, Netherlands

The ORCID identification number(s) for the author(s) of this article can be found under https://doi.org/10.1002/adma.202006109.

DOI: 10.1002/adma.202006109

reverse bias, effectively decreasing the rate of charge transport by reverting to non-resonant tunneling (the tunneling part of tunneling–hopping).[27] Although the fragility of the thiol-SAMs precluded the confirmation of the tunneling–hopping mechanism by variable-temperature measurements, evidence suggests that is the same well-established mechanism by which ferrocenes rectify, except the polarity is reversed because unoccupied orbitals mediate the bias-dependent, thermally activated processes rather than occupied orbitals.[28]

Here, we establish that the GE phase in the SAMs of **PTEG-1** serves as an efficient tunneling medium, but does not effect rectification and that both ferrocene (**FcTEG**) and fullerene moieties can be exchanged into the SAB to form GESAMs (i.e., SABs in which the top layer is exchanged for another GE); in both cases, rectification is mediated by the frontier orbitals of the moiety, which we were able to confirm with variable-temperature measurements due to the robustness of SABs. The absence of rectification induced by the GE phase suggests that the dipoles arising from the polar C—O bonds are either too disordered or insufficient in magnitude to effect rectification via mechanism (3), but further study is needed to ascertain the precise ordering of the chains and conformation-dependent phenomena such as odd–even effects and the influence of dipoles on the rate of charge transport.[29,30] Tunneling junctions comprising GESAMs of **PTEG-1** and **FcTEG** produce distinctively different rectification ratios ($R = |J(+)|/|J(-)|$, where J is current density) that are in good agreement with literature vis-á-vis which frontier orbitals participate in the thermally-activated processes that lead to rectification (i.e., mechanism (4) above).[24,27] By utilizing the surface tension of EGaIn top electrodes, we demonstrate in operando modulation of rectification in reconfigurable molecular junctions comprising SABs of **PTEG-1**. Furthermore, by incorporating junctions into microfluidic channels, we were able to leverage this novel form of in situ switching to encode stochastic data in chemical packets (in the form of droplets) to form solid-state memory. This rudimentary stochastic computing demonstrates the potential for molecular (tunneling) junctions to process information in the form of probabilities,[31,32] facilitating the development of useful molecular-electronic computation with intrinsic fault-tolerance.

We formed SABs of **PTEG-1** by immersing freshly prepared, ultrasmooth, template-stripped (TS) Au substrates (Au^{TS}) into a toluene solution of **PTEG-1** for 24 h (see Experimental Section for details). The free **PTEG-1** molecules in solution first formed a self-assembled monolayer (SAM) on Au^{TS} via chemisorption of the fullerene cage, followed by the growth of a second layer of **PTEG-1** on top of the bottom layer via dipole–dipole interactions between interdigitating GE chains (**Figure 1**a).[18] To form SAMs of **PTEG-1**, we rinsed the SABs of **PTEG-1** with toluene to remove only the top layer, exposing the densely-packed, chemisorbed monolayer of **PTEG-1**. To form GESAMs of **FcTEG** (on **PTEG-1**, see the Supporting Information text, Figure S1–S3 and Figure S24, Supporting Information for synthesis and characterization), we exchanged the top layer of the SABs of **PTEG-1** with **FcTEG** by immersing the SABs in a toluene solution of **FcTEG** for 24 h. The three samples exhibited distinct surface morphologies by atomic force microscopy (AFM), with roughness of 0.455 nm for SAMs of **PTEG-1**, 0.435 nm for SABs of **PTEG-1** and 0.185 nm for GESAMs of **FcTEG** (Figure S25, Supporting Information). The water contact angle of the GESAMs of **FcTEG** (74°) confirms that the top layer of **PTEG-1**, which has a contact angle of 68°, is replaced by **FcTEG** and that the exchange process does not result in a SAM of **PTEG-1**, which has a contact angle of 45° (Table S3, Supporting Information) or a monolayer of **FcTEG** in which the ferrocene moiety acts as anchoring group. We further confirmed the transitions from SABs of **PTEG-1** (11.9 to 13.4 Å) to SAMs of **PTEG-1** (25.1 to 27.0 Å) and GESAMs of **FcTEG** (21.5 to 22.2 Å) by measuring their respective thicknesses using ellipsometry and angle-resolved X-ray photoelectron spectroscopy (AR-XPS); these data are summarized in Tables S2, S4, and S5, Supporting Information. Moreover, the XPS spectra of the SABs of **PTEG-1** and the GESAMs of **FcTEG** in Figure S27, Supporting Information show that the C—C (284.5 eV), C=C/C—N (285.9 eV) and C—O (288.7 eV) peaks of the C 1s region and the O—C (532.0 eV) peaks of the O 1s region are in good agreement with the spectra of the SAMs of **PTEG-1**, further confirming the presence of the **PTEG-1** anchoring layer after exchange. The peaks of $Fe2p_{3/2}$ (707.9 eV) and $Fe2p_{1/2}$ (720.83 eV) in the XPS spectrum of the **FcTEG** GESAMs (Figure S27i, Supporting Information) are in perfect agreement with the literature[33] and indicate that **FcTEG** exchanges with the SABs of **PTEG-1** to form the target GESAMs on **PTEG-1**.

We characterized the charge transport properties of the SAMs of **PTEG-1** and the GESAMs of **PTEG-1** and **FcTEG** (which differ from the SABs of **PTEG-1** only in that they are formed by exchange subsequent to the initial SAB formation, as described above) by contacting them with conical tips of eutectic gallium indium (EGaIn)[34] or Au-coated AFM tips (Au^{AFM}) to form junctions with the structure Au^{TS}/(GE)SAM//EGaIn or Au^{TS}/(GE)SAM/Au^{AFM} where "/" denotes interfaces defined by chemisorption and "//" by physisorption. We used these high-throughput techniques to help elucidate the charge transport properties of the self-assemblies in tunneling junctions without the need to fabricate devices. We found a significantly higher conductance from the SAMs of **PTEG-1** than the GESAMs of **PTEG-1** and **FcTEG** in both EGaIn and conductive probe AFM (CP-AFM) junctions (Figure 1b,d), which is in good agreement with our previous observations[18] and reflects the sensitivity of tunneling charge transport properties to thickness. The absolute currents flowing through CP-AFM junctions comprising the GESAMs of **PTEG-1** and **FcTEG** exceed the dynamic range of the opamps of CP-AFM at low biases, hence we plotted their I–V curves in linear scale for comparison over electrical conductance. As we extended the bias window, the junctions comprising GESAMs of **PTEG-1** and **FcTEG** produced asymmetric J–V curves with opposite dependence on bias, for example, $|J(+)| > |J(-)|$ for GESAMs of **PTEG-1** and $|J(+)| < |J(-)|$ for GESAMs of **FcTEG** (Figure 1b). The difference is most prominent at ±1.5 V, where the conductance of the GESAMs of **PTEG-1** is almost the same as that of SAMs of **PTEG-1** at 1.5 V, but significantly lower at −1.5 V. The conductance of the GESAMs of **FcTEG** exhibited the same trend, but with opposite dependence on bias. The rectification ratios ($R = |J(+)|/|J(-)|$) reach a maximum of $R = 88$ for the junctions comprising GESAMs of **PTEG-1** and a minimum of $R = 6.9 \times 10^{-3}$ for the junctions comprising GESAMs of **FcTEG** (Figure 1c). These values are comparable to that of conventional SAMs of fullerene/ferrorcene-functionalized alkanethiols.[24,27,35] The results from CP-AFM junctions are in good agreement with those from EGaIn junctions (Figure 1d,e); the differences in the

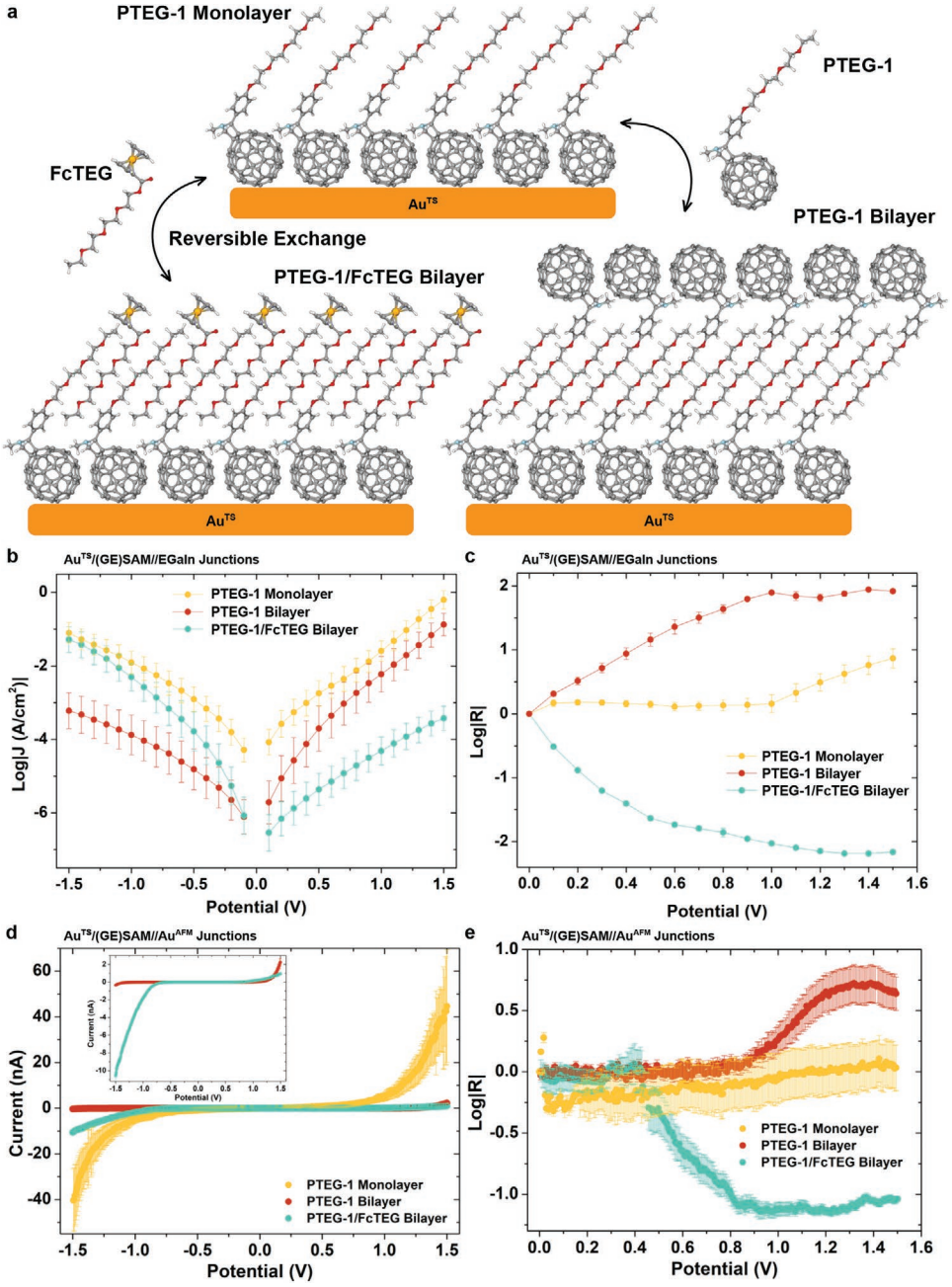

Figure 1. Characterization of the self-assembled monolayers and bilayers of **PTEG-1** and **FcTEG**. a) A schematic of the transition from a self-assembled monolayer of **PTEG-1** into the bilayers of **PTEG-1** and **PTEG-1**/**FcTEG** via reversible exchange. b) Plots of log|*J*| versus potential for Au^{TS}/**PTEG-1**//EGaIn, Au^{TS}/**PTEG-1**//**PTEG-1**//EGaIn and Au^{TS}/**PTEG-1**//**FcTEG**//EGaIn junctions. c) Plots of log|*R*| versus potential of Au^{TS}/**PTEG-1**//EGaIn, Au^{TS}/**PTEG-1**//**PTEG-1**//EGaIn and Au^{TS}/**PTEG-1**//**FcTEG**//EGaIn junctions. d) Plots of *I* versus potential for Au^{TS}/**PTEG-1**//Au^{AFM}, Au^{TS}/**PTEG-1**//**PTEG-1**//Au^{AFM} and Au^{TS}/**PTEG-1**//**FcTEG**//Au^{AFM} junctions. Enlarged *I*–*V* curves of Au^{TS}/**PTEG-1**//**PTEG-1**//Au^{AFM} and Au^{TS}/**PTEG-1**//**FcTEG**//Au^{AFM} junctions are shown in the inset. e) Plots of log|*R*| versus potential of Au^{TS}/**PTEG-1**//Au^{AFM}, Au^{TS}/**PTEG-1**//**PTEG-1**//Au^{AFM} and Au^{TS}/**PTEG-1**//**FcTEG**//Au^{AFM} junctions. The error bars are the 95% confidence intervals.

onset of rectification are consistent with our previous work comparing EGaIn and CP-AFM data.[27] Interestingly, the EGaIn junctions comprising the SAMs of **PTEG-1** exhibited slightly asymmetric *J*–*V* curves ($R < 10$ at 1.5 V), while the CP-AFM junctions of the SAMs exhibited symmetric *I*–*V* curves.

There are two components to elucidating the mechanism of rectification: 1) the role of GE chains in the charge transport properties of the self-assemblies and 2) the mechanism of charge transport in the tunneling junctions comprising the GESAMs of **PTEG-1** and **FcTEG**. To evaluate the role of the GE chains, we grew two series of SAMs, one from fullerenes bearing GE chains (**FP-EG*n***, $n = 2, 3, 4, 5$, where **PTEG-1** corresponds to $n = 3$; see Supporting Information and Figures S4 and S5, Supporting Information for synthesis and characterization)

and one from fullerenes bearing alkyl chains (**FP-C*n***, n = 5, 7, 9, 11; see Supporting Information and Figures S6–S23, Supporting Information for synthesis and characterization) on Au^{TS}, among which **PTEG-1** and **FP-C11** have the same number of (non-hydrogen) atoms in the backbones of the GE/alkyl chains. Surface morphology measured by AFM confirmed the formation of monolayers instead of SABs (Figure S25, Supporting Information). We measured the dependence of the electrical conductance of the SAMs of **FP-EG*n*** and **FP-C*n*** on the lengths of the molecules they comprise by forming Au^{TS}/**FP-EG*n*** (or **FP-C*n***)//EGaIn (or Au^{AFM}) junctions, which is summarized in **Figure 2**. We observed a decrease in conductance with increasing lengths of the GE chains attached to the fullerene cages in the **FP-EG*n*** SAMs and the analogous alkyl chains in the **FP-C*n*** SAMs in both EGaIn (Figure 2a,b) and CP-AFM junctions (Figure 2d,e). Figure 2c,f show this exponential dependence of J (from EGaIn junctions) and I (from CP-AFM junctions) on the number of (non-hydrogen) atoms in the GE/alkyl chains (that is, carbon/oxygen for **FP-EG*n***, carbon for **FP-C*n***), from which we extracted the tunneling decay coefficient β using the equation $J = J_0 e^{-\beta d}$, where d is the width of the tunneling barrier, in this case defined by molecular-length, and J_0 is the theoretical value of J when $d = 0$. We measured β at ±0.5 V and ±1 V from EGaIn junctions and ±1 and ±1.5 V from CP-AFM junctions. We found $\beta = 0.26$ atom^{-1} in EGaIn junctions and $\beta = 0.40$ atom^{-1} in CP-AFM junctions for **FP-EG*n*** SAMs; $\beta = 1.08$ atom^{-1} in EGaIn junctions and $\beta = 0.94$ atom^{-1} in CP-AFM junctions for **FP-C*n*** SAMs (Figure 2c,f). The consensus value of β at ±0.5 V for tunneling junctions comprising alkanethiols on Au^{TS} is ≈1.10 atom^{-1} (Figure S28, Supporting Information).[36] A similar value of β from the SAMs of **FP-C*n*** indicates the dominant mechanism of charge transport is nonresonant tunneling through *trans*-extended alkyl chains, while the fullerene cage acts as an anchoring group, analogous to sulfur in thiol-SAMs.[18] It also confirms that the alkyl chains are sufficiently densely-packed to define a tunneling barrier. The observation of a lower value of β for SAMs of **FP-EG*n*** than for SAMs of **FP-C*n*** is commensurate with previous studies in which the authors ascribe the lower value of β for EG chains to superexchange coupling between the lone pairs on neighboring oxygen atoms.[37] The alignment of dipole moments has also been shown to influence the rate of tunneling charge transport, which may explain the subtle differences in the J–V characteristics.[29,30] A similar explanation for SAMs of **FP-EG*n*** is plausible, given the comparable values of β for both the alkyl- and GE-functionalized fullerenes to their thiol counterparts. The evolution of J for both Au^{TS}/**PTEG-1**//**PTEG-1**//EGaIn junctions and Au^{TS}/**PTEG-1**//**FcTEG**//EGaIn junctions under varying temperature prove that the tunneling–hopping mechanism, mediated by the frontier states of the ferrocene and fullerene moieties from the top layer, is responsible for the generation of rectification as summarized in Figure S37, Supporting Information and in good agreement with studies on thiol-SAMs.[24,27] (As discussed above, the term tunneling–hopping refers to the coexistence of tunneling and a thermally activated hopping process and not a transition between pure tunneling and

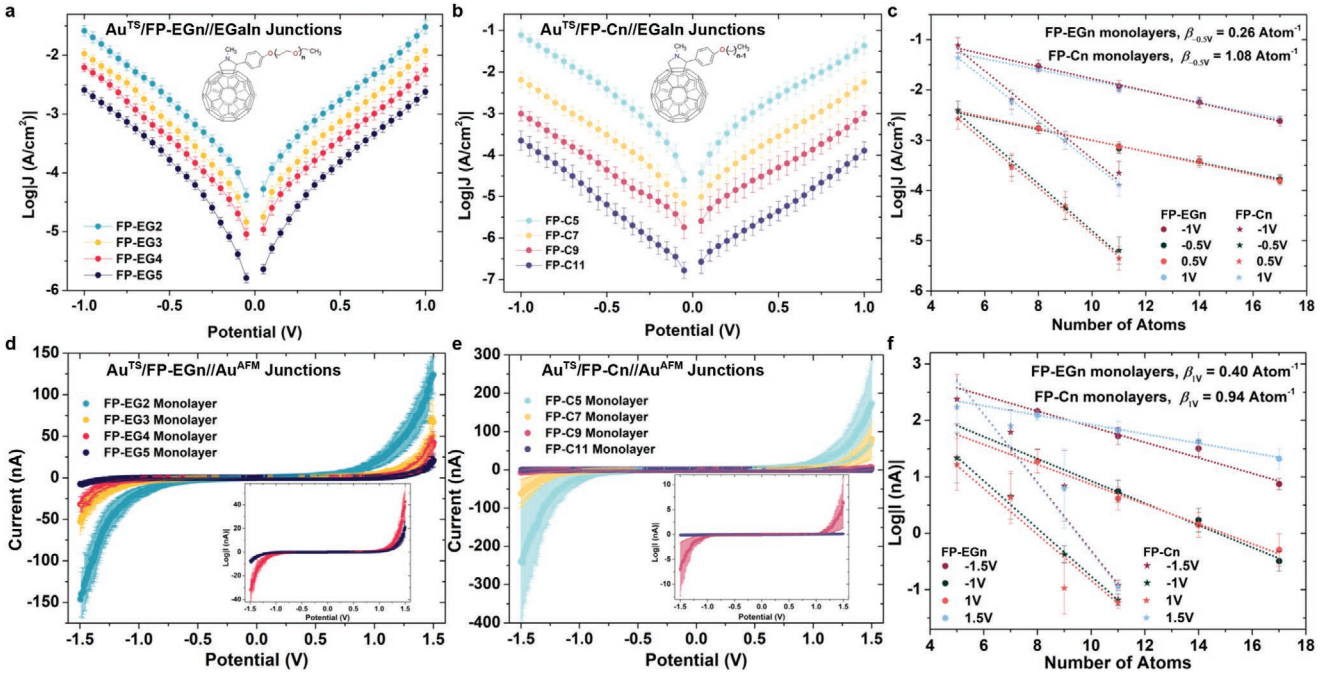

Figure 2. Characterization of the charge transport properties of the self-assembled monolayers of **FP-EG*n*** (n = 2, 3, 4, 5) and **FP-C*n*** (n = 5, 7, 9, 11). a,b) Plots of log|J| versus potential of Au^{TS}/**FP-EG*n***//EGaIn (a) and Au^{TS}/**FP-C*n***//EGaIn (b) junctions. c) Plots of log|J| determined at –1, –0.5, 0.5, and 1 V in EGaIn junctions versus the number of non-hydrogen atoms in oligoGEs of **FP-EG*n*** molecules and in the alkyl chains of **FP-C*n*** molecules (the oxygen attached to the phenyl group is not counted). d,e) Plots of I versus potential of Au^{TS}/**FP-C*n***//Au^{AFM} (d) and Au^{TS}/**FP-C*n***//Au^{AFM} (e) junctions. Enlarged I–V curves of the two longer molecules from both junctions are shown in the insets. f) Plots of log|I| determined at –1.5, –1, 1, and 1.5 V in CP-AFM junctions versus the number of non-hydrogen atoms in the oligoGEs of **FP-EG*n*** molecules and in the alkyl chains of **FP-C*n*** molecules (the oxygen attached to the phenyl group is not counted). The error bars are the 95% confidence intervals. The dotted lines are linear fits to the data points.

pure hopping.[28]) The activation energies of the hopping processes ((69.04 ± 3.14) meV for Au^{TS}/**PTEG-1**//**PTEG-1**//EGaIn junctions and (57.54 ± 3.63) meV for Au^{TS}/**PTEG-1**//**FcTEG**//EGaIn junctions) reflect the barrier to charge-injection at the GESAM//EGaIn interface (see Supporting Information for details).[38] Together, these experiments confirm that the mechanism of rectification in thiol-SAMs is generalizable and applicable to GESAMs and that the presence of GE chains does not significantly affect charge transport.

While it is important to verify the mechanism of rectification in GESAMs, the ability of fullerenes and ferrocenes to affect rectification is not new; however, combined with the unique properties of GESAMs, these molecules can be used to modulate rectification while a junction is being observed under bias. This in operando control over the properties of a tunneling junction is a technological step forward from in situ and in-place modulation[9] and, unlike conductance-switching,[8] is unique to molecular tunneling junctions. To allow for exchange in assembled Au^{TS}/**PTEG-1**//**PTEG-1**//EGaIn junctions, we formed them by contacting the GESAMs of **PTEG-1** with conical EGaIn tips in a microfluidic channel with precise control over back pressure (see Experimental Section for details), as shown in **Figure 3**a,b; the junction is situated in the semicircular opening of the channel in the inset of Figure 3b. We then injected neat toluene or a toluene solution of **PTEG-1** into the channel to immerse the junction completely at a rate of 1 mL h^{-1} for 20 s, followed by an air flow for 40 s to remove the excess liquid. Once a junction was formed, all components, including the syringe, EGaIn tip, substrate, and microfluidic channel remained static throughout the experiments. We performed ten cycles of neat toluene → **PTEG-1** solution on 20 junctions. The resulting *J*–*V* curves are summarized in Figure 3c. We observed a reversible transition from asymmetric *J*–*V* curves corresponding to GESAMs of **PTEG-1**, both in conductance and the direction of rectification, to symmetric *J*–*V* curves corresponding to SAMs of **PTEG-1** and vice versa. The evolution of log|*R*| (i.e., the rectification ratio on a logarithmic scale) measured at 1 V in Figure 3d shows the switching between the GESAMs of **PTEG-1** (log|*R*| ≈ 2.5) and the SAMs of **PTEG-1** (log|*R*| ≈ 0.2) with an on/off ratio of 200 over ten cycles in 20 min. Control junctions of Au^{TS}/**PTEG-1**//**PTEG-1**//EGaIn measured with air flow, but in the absence of toluene or **PTEG-1**, resulted in an invariant log|*R*| ≈ 2.5, proving that rectification is affected by exposure to neat toluene and the toluene solutions of **PTEG-1**. As shown in Figure 3a, we hypothesize that in operando switching from high log|*R*| to low log|*R*| occurs because toluene reversibly dewets EGaIn from the (GE)SAMs of **PTEG-1**; neat toluene removes the top layer of **PTEG-1** converting a GESAM (back) to a SAM, while the solutions of **PTEG-1** restore the top layer converting a SAM back to a GESAM.

For further insight into the role of dewetting, we formed Au^{TS}/**PTEG-1**//EGaIn junctions by contacting SAMs of **PTEG-1** with conical EGaIn tips in a microfluidic channel and recorded their *J*–*V* curves in three states: 1) before the injection of toluene, 2) with the junctions completely immersed in toluene, and 3) after the removal of toluene (Figure S30b, Supporting Information). Figure S30c, Supporting Information showed almost indistinguishable *J*–*V* curves, corresponding to the

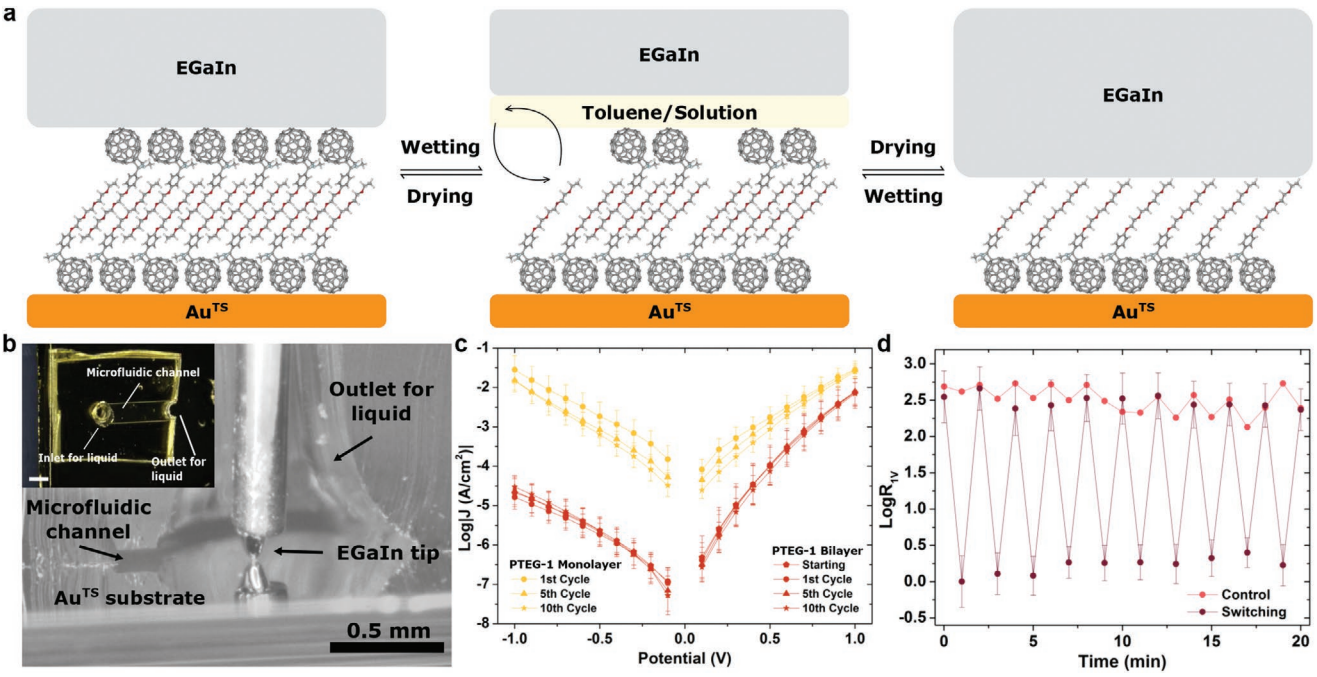

Figure 3. Characterization of the in operando modulation of rectification in EGaIn junctions. a) A schematic showing the transition between **PTEG-1** monolayer and bilayer in a EGaIn junction in the presence of toluene or **PTEG-1** solution. b) The structure of the junction for in operando modulation of rectification under optical microscopy. The inset is a zoomed-out image of the microfluidic channel on Au^{TS} substrate. The scale bar of the inset is 1 mm. c) Plots of log|*J*| versus potential of Au^{TS}/**PTEG-1**//EGaIn junctions over ten cycles of in operando modulation. d) The evolution of log|*R*| at 1 V of Au^{TS}/**PTEG-1**//EGaIn junctions over ten cycles of in operando modulation over 20 min, in comparison to control. The error bars are the standard deviations of the means.

SAMs of **PTEG-1**, of the junctions in (1) and (3), but significantly lower conductance in (2). These results suggest that the EGaIn electrodes were in contact with the SAMs in (1) and (3) and that the effective contact area did not differ, but that in state (2) the EGaIn detached, at least partly, from the SAM; i.e., in the presence of toluene EGaIn dewets from the SAM and that, when it rewets in the absence of toluene, the contact area is restored, suggesting a process that is governed by interfacial free-energy. Using the Young–Laplace equation, we calculated the contact angle at the toluene/EGaIn interface in the junctions to be 87.5°, meaning it is energetically favorable for toluene to dewet EGaIn from the SAMs of **PTEG-1** (see Supporting Information for details). Varying the SAM/solvent and SAM/EGaIn interfaces by repeating the experiment on EGaIn junctions comprising SAMs of hexadecanethiolate (SC16) produced similar results (Figure S1, Supporting Information), but with more junction-to-junction variance in conductance, supporting the hypothesis that the regeneration of the junctions depends entirely on the interfacial free-energies between toluene, EGaIn and the SAM. (The increase in variance is most likely a manifestation of the fragility of thiol-SAMs.) Although we could not observe the details of how EGaIn tips deform and regenerate or possible changes in the packing of the SAMs, the data strongly support a reversible process in which EGaIn reversibly contracts and dewets in the presence of toluene and returns to its original shape upon removal of toluene (Figure S30a, Supporting Information).

While robust, in-place conductance switching has obvious applications in memory[3] and the spatial encoding of (binary) data,[39] in operando switching provides the opportunity to interact with bitstreams in a manner that leverages the unique properties of molecular tunneling junctions. In information theory, the maximum rate at which information can flow though a channel is limited by noise, which is often referred as the Shannon limit.[40] In practice, this theory defines the efficiency of compression and error-correction schemes on linear bitstreams, in which numbers are represented by the precise ordering of bits, the integrity of which is verified by the inclusion of additional information such as checksums;[41] if a pre-defined length of bits fails a check it must be corrected or retransmitted. In stochastic computing, numbers are represented by probabilities of bits rather than exact sequences.[31] For example, instead of representing $\frac{1}{3}$ as a decimal number encoded in a fixed-length string of bits in a precise order, it is encoded in a bitstream of arbitrary length and order in which $\frac{1}{3}$ of the bits are 1's, making it tolerant to bit-flips (i.e., errors). Thus, stochastic computing is a method for transmitting data near the Shannon Limit without the overhead of correction and retransmission, which is useful for neural networks that process information through layers of weighted probabilistic nodes, rather than the standard von Neumann architecture where linear bitstreams are continuously transmitted between memory and processing units. Although stochastic computing can be simulated in software, only hardware implementations can realize these advantages. In our implementation, trains of droplets form bitstreams that are read out by Au^{TS}/**PTEG-1**// EGaIn junctions. Since the state of the junction is entirely defined by interfacial free-energies, the timing and direction of the bitstream do not matter and the system can be started and stopped without affecting its state; conventional computation requires constant power and a clock to synchronize operations to registers. As shown in **Figure 4**a, the presence or absence of **PTEG-1** in toluene droplets defines bits in chemical packets that are compartmentalized by air barriers (bubbles). These droplets define the state of EGaIn junctions by affecting their composition (denoted as a TRANSFER operation), which can be read out either as a rectification ratio (which is self-referencing) or a conductance (threshold) from the junctions to complete a READ operation, translating information encoded in chemical packets to electrical signals.

Rather than relying on conical tips, we fabricated 150 μm-wide EGaIn microelectrodes confined between arrays of periodically-positioned posts using the reported method[42,43] (Figure 4b) to form crossbar junctions comprising GESAMs of **PTEG-1** with Au^{TS} bottom electrodes (50 μm wide) flanked by 450 μm-wide microfluidic channels that deliver chemical packets to modulate the conductance of junctions. We defined an 8-bit register from eight junctions, each of which functions as a memory bit, such that an 8-bit string could be read out from the values of $\log|J|$ measured at −1 V. High-conductance states, defined by a junction comprising a SAM, represent 1's and low-conductance states, defined by a junction comprising a GESAM, represent 0's. (The additional microfluidic channels in Figure 4a are necessary to stabilize the central channels that define the 8-bit register.) All strings started with all memory bits (junctions) in 0 states because they were formed from pristine GESAMs of **PTEG-1**. To change the state of a memory bit in a TRANSFER operation, we delivered chemical packets to the corresponding junction by injecting droplets of toluene to set a 1 or toluene solution of **PTEG-1** to set a 0. Measuring the current through the junction completes the READ operation. We chose $\log|J|$ at −1 V as the observable to differentiate bits to stress the in operando nature of the register—i.e., with a constant bias of −1 V applied to the EGaIn electrode, the current changes in real time as subsequent TRANSFER and READ operations modulate the state of the register. (Measuring $\log|R|$, which is shown in Figure S34, Supporting Information is, in principle, more robust because it is self-referencing, obviating the need to define a threshold current, but it necessitates applying at least two different biases to the junctions for each READ operation.) Figure 4c summarizes the evolution of $\log|J|$ as the state of each memory bit changes in response to different chemical packets in two, separate 8-bit registers (i.e., two microfluidic chips comprising crossbar junctions) throughout two full TRANSFER/READ operations in comparison to two control registers on which only the READ operation was performed (Figure S33, Supporting Information). The memory bits showed a clear distinctions between the 1 and 0 states in their distribution of $\log|J|$ (Figure 4d), which is in good agreement with the *J–V* characteristics of the SAMs and GESAMs of **PTEG-1** in EGaIn junctions (Figure 1b). The distinction between states is resolvable down to a READ bias of −0.1 V (Figure S35, Supporting Information), highlighting their potential energy efficiency.

To demonstrate rudimentary stochastic computation, we encoded numbers into 8-bit strings (i.e., chemical packets of either neat toluene or solutions of **PTEG-1**) probabilistically and fed them through a register. In the examples shown in

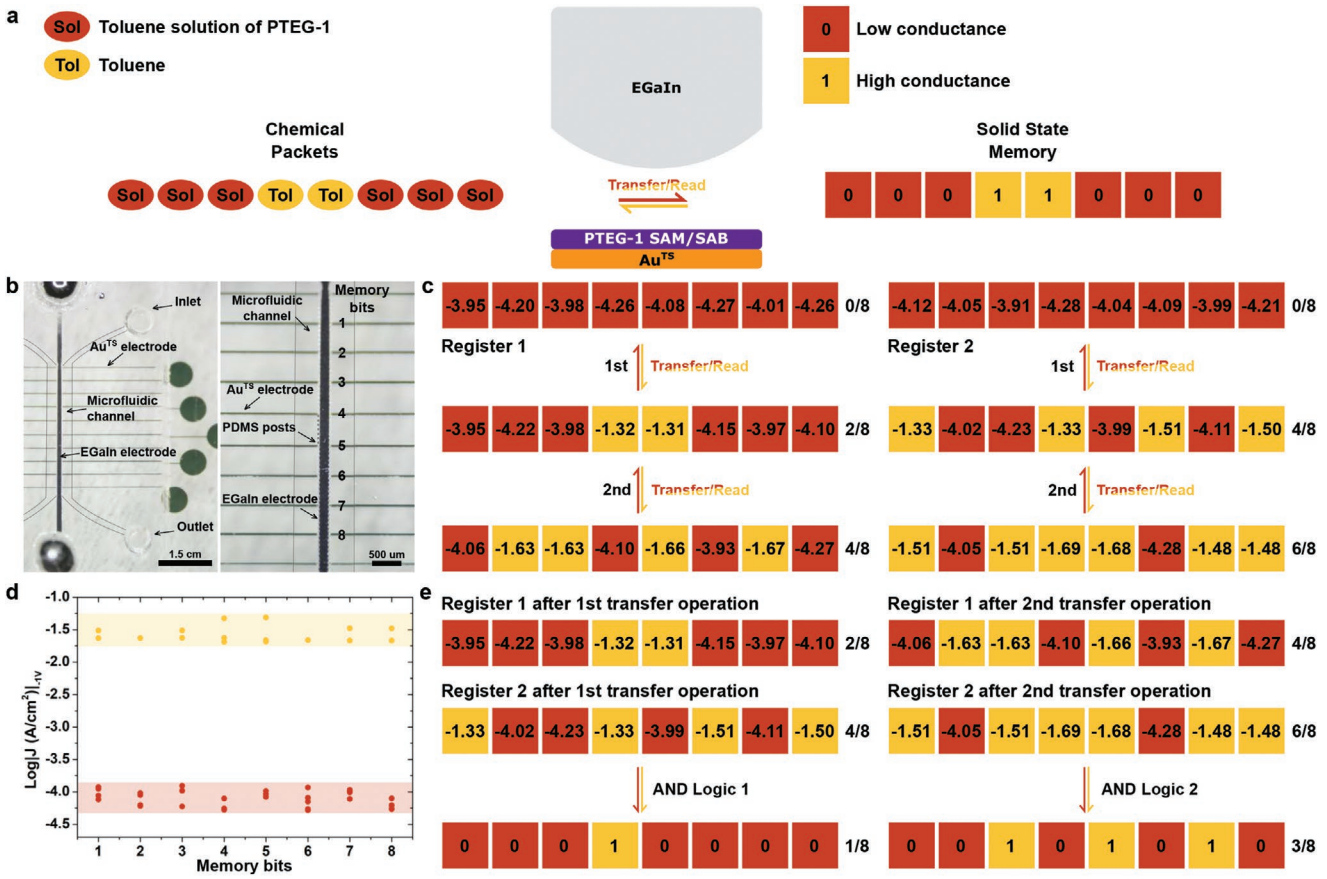

Figure 4. Stochastic computation using two bit strings fabricated from Au^{TS}/**PTEG-1**//**PTEG-1**//EGaIn crossbar junctions in microfluidic channels. a) A schematic showing the translation between liquid state input and solid state output in Au^{TS}/**PTEG-1**//**PTEG-1**//EGaIn crossbar junctions in operando. b) Photographs of an 8-bit register. We positioned EGaIn microelectrode orthogonally to the Au^{TS} electrodes to form crossbar junctions that define the memory bits of the register. The photograph on the right is a zoomed-in image of the left image. c) A schematic showing the changes in the current density of each memory bit of the two registers (register 1 on the left and 2 on the right) before and after two TRANSFER operations. The numbers are current densities at –1 V in logarithmic scale (log|*J*| [A cm^{-2}]|). Red and yellow were assigned to represent off and on states of the memory bits. d) The distribution of the current densities at –1 V of all memory bits in the two TRANSFER operations. e) A schematic showing stochastic computation using the two bit strings after two TRANSFER operations.

Figure 4e, we encoded $\frac{1}{4}$ as {0, 0, 0, 1, 1, 0, 0, 0}, $\frac{1}{2}$ as either {1, 0, 0, 1, 0, 1, 0, 1} or {0, 1, 1, 0, 1, 0, 1, 0}, and $\frac{3}{4}$ as {1, 0, 1, 1, 0, 1, 1}. Multiplying the strings stored in the registers using AND gate logic resulted in the probabilities shown in Equation (1), which give the correct answers: $\frac{1}{4}\times\frac{1}{2}=\frac{1}{8}$ and $\frac{1}{2}\times\frac{3}{4}=\frac{3}{8}$.

$$1.\ \{0,0,0,1,1,0,0,0\}\,\&\,\{1,0,0,1,0,1,0,1\}=\{0,0,0,1,0,0,0,0\}\equiv\frac{1}{8}$$
$$2.\ \{0,1,1,0,1,0,1,0\}\,\&\,\{1,0,1,1,1,0,1,1\}=\{0,0,1,0,1,0,1,0\}\equiv\frac{3}{8} \quad (1)$$

The representation of probability was neither limited to a certain arrangement of bits, as representing $\frac{1}{2}$ as {1, 0, 0, 1, 0, 1, 0, 1} and {0, 1, 1, 0, 1, 0, 1, 0} both gave the correct answer, nor the length of the string, which is defined by the length of the register (i.e., the number of crossbar junctions); increasing the length of the register only improves accuracy and error-tolerance. Although the AND operation was performed by hand, these results demonstrate that the robustness and fidelity of the GESAM ⇌ SAM interconversion is sufficient to perform multiple logical operations that effectively convert information stored in microfluidic droplets into electrical signals.

The usefulness of molecular tunneling junctions, particularly in the context of integration with existing integrated circuits, is ultimately constrained by the stability of tunneling junctions and the ability to change their properties with external inputs. Single-molecule junctions are transient by nature and SAMs of thiols are fragile; however, GESAMs are air-stable and sufficiently mechanically robust to undergo self-assembly in operando to change their composition, creating a platform to realize the incredible gamut of control afforded by Chemistry in fieldable devices. Using only two compounds, we have shown devices that can interconvert between resistor and diode with control over the direction and magnitude of rectification and, while similar outputs can be realized using field-effect transistors, GESAMs accomplish it by physically converting between fundamental circuit elements that retain their states when power is interrupted. Using the same concept, we constructed 8-bit registers capable of reading information with sufficient fidelity to perform stochastic computing by converting

information stored in chemical packets as microfluidic droplets to electrical signals. Each memory bit functions like a memristor in that its electrical output depends on the past history of exposure to chemical packets and its state is not lost when it is de-energized, meaning the timing and direction of the chemical packets do not matter. Also, because its electrical output is defined by its composition, the concepts demonstrated in this paper could be extended to any process capable of generating chemical signals and is not limited to stochastic computation. The underlying principle is the self-assembly of GESAMs, meaning that virtually any compound functionalized with a GE tail can be incorporated and, for example, the electrical properties of the memory bits could be used for sensing or dosimetry or combined with photo-switches for non-binary logic.

Experimental Section

*Preparation of Monolayers and Bilayers of **PTEG–1***: Self-assembled monolayers and bilayers of **PTEG–1** were prepared by incubating freshly cleaved 1×1 cm^2 Au^{TS} surfaces for 24 h in 1.2 mL of 0.5×10^{-3} M solutions in toluene at room temperature. To form monolayers, the substrates were rinsed gently with toluene (3×1 mL) and residual solvent on surface was removed by gently blowing N_2. To form bilayers, the substrates were taken out of the solution and rinsed gently with toluene (0.5 mL), the residual solvent was gently blown away by N_2.

*Preparation of Bilayers of **PTEG–1/FcTEG***: Self-assembled bilayers of **PTEG–1/FcTEG** were prepared through exchange of **PTEG–1** from its pristine bilayer with **FcTEG** over two steps. First, bilayers of **PTEG–1** were formed by incubating freshly cleaved 1×1 cm^2 Au^{TS} surfaces for 24 h in 1.2 mL of 0.5×10^{-3} M solutions in toluene at room temperature. The substrates were then incubated for 24 h in 5 mL of 5×10^{-3} M solution of **FcTEG** in toluene at room temperature. After incubation, they were taken out of the solution, gently rinsed with toluene (0.5 mL) and the residual solvent was blown away by N_2.

EGaIn Measurement: The electrical measurement with EGaIn, as well as sample preparation and handling, was performed under ambient conditions. In the measurement, the sample was grounded and the EGaIn was biased. At least three samples were examined for monolayers/bilayers. The potential windows include the following: 1) 0 V → 1 V → –1 V → 0 V, steps of 0.05 V; (2) 0 V → 1.5 V → –1.5 V → 0 V, steps of 0.1 V. A total of five trace/retrace cycles were recorded for each junction, and shorts that occurred during the measurement (short upon contact with a bias of 1 V or during the cycle) were counted for the failure of junction.

In Operando Modulation: For modulation in EGaIn junctions with conical tips, liquid toluene or a toluene solution of **PTEG–1** (0.5×10^{-3} M) was injected into the microfluidic channel using syringe pumps at a rate of 1 mL h^{-1} for 20 s. Then an air flow was introduced into the microfluidic channel by syringe for 40 s to remove toluene or the solution. The EGaIn conical tips were formed using a syringe with precise pressure control (pulse pressure 30.0 kPa, back pressure 1.30 kPa, EFD Ultimus V, Nordson). For modulation in EGaIn cross-bar junctions, the droplets of toluene or the toluene solution of **PTEG–1** (0.5×10^{-3} M) were injected into the microfluidic channels (treated with oxygen plasma for 1 min and sequentially in the fume of trichloro(1H,1H,2H,2H-perfluorooctyl) silane at low pressure in a desiccator for 30 min) through a customized Y-junction connected to two separate syringe pumps (Fusion 200, Chemyx, UK and NE-4000, New Era Pump Systems, Inc. USA) via PTFE tubing at a rate 0.05 mL h^{-1} (different flow rate between 0.01–0.05 mL h^{-1} could be chosen to produce a stable droplet train for individual sample). After the droplets were successfully delivered to the specific junctions, the injection was stopped for 1 min and immediately replaced by a stream of air for 4 min to remove the solvent or the solution.

AFM Measurement: Conductive probe AFM (CP-AFM) was performed on a Bruker AFM Multimode MMAFM-2 equipped with a PeakForce TUNA application module (Bruker). In CP-AFM measurements, samples fabricated on Au^{TS} substrates were contacted with an Au-coated silicon nitride tip with a nominal radius of 30 nm (NPG-10, Bruker, tip A: resonant frequency 65 kHz, spring constant: 0.35 N m^{-1}) in TUNA mode with load force of 1.4 nN. The AFM tip was grounded and the sample was biased from –1.5 to +1.5 V and from +1.5 to –1.5 V to record the *I–V* curves (512 data points per trace were taken): a maximum of 20 trace/retrace cycles per junction were performed. After every junction, the tip was withdrawn and moved to a different spot, and engaged again for a total of 50 junctions over three samples analyzed. Between different samples a new tip was used. The data were analyzed with the same software used for EGaIn using the current *I* instead of the current density *J*.

Supporting Information

Supporting Information is available from the Wiley Online Library or from the author.

Acknowledgements

This work is part of the research program of the Foundation for Fundamental Research on Matter (FOM), which is part of The Netherlands Organization for Scientific Research (NWO). This is a publication by the FOM Focus Group "Next Generation Organic Photovoltaics", participating in the Dutch Institute for Fundamental Energy Research (DIFFER). R.C.C. and X.Q. acknowledge the Zernike Institute of Advanced Materials for financial support. G.Y. also acknowledges the Chinese Scholarship Council.

Conflict of Interest

The authors declare no conflict of interest.

Keywords

in operando reconfiguration, molecular diodes, molecular electronics, microfluidics, self-assembly

Received: September 7, 2020
Revised: October 27, 2020
Published online: December 16, 2020

[1] R. F. Service, *Science* **2014**, *345*, 614.
[2] M. Carlotti, A. Kovalchuk, T. Wächter, X. Qiu, M. Zharnikov, R. C. Chiechi, *Nat. Commun.* **2016**, *7*, 13904.
[3] Y. Han, C. Nickle, Z. Zhang, H. P. A. G. Astier, T. J. Duffin, D. Qi, Z. Wang, E. Barco, D. Thompson, C. A. Nijhuis, *Nat. Mater.* **2020**, *19*, 843.
[4] Y. Kim, A. Garcia-Lekue, D. Sysoiev, T. Frederiksen, U. Groth, E. Scheer, *Phys. Rev. Lett.* **2012**, *109*, 1.
[5] K. Smaali, S. Lenfant, S. Karpe, M. Oçafrain, P. Blanchard, D. Deresmes, S. Godey, A. Rochefort, J. Roncali, D. Vuillaume, *ACS Nano* **2010**, *4*, 2411.
[6] N. Darwish, A. C. Aragonès, T. Darwish, S. Ciampi, I. Díez-Pérez, *Nano Lett.* **2014**, *14*, 7064.
[7] S. Kumar, J. T. van Herpt, R. Y. N. Gengler, B. L. Feringa, P. Rudolf, R. C. Chiechi, *J. Am. Chem. Soc.* **2016**, *138*, 12519.
[8] C. Jia, A. Migliore, N. Xin, S. Huang, J. Wang, Q. Yang, S. Wang, H. Chen, D. Wang, B. Feng, Z. Liu, G. Zhang, D.-h. Qu, H. Tian, M. A. Ratner, H. Xu, A. Nitzan, X. Guo, *Science* **2016**, *352*, 1443.

[9] Y. Ai, A. Kovalchuk, X. Qiu, Y. Zhang, S. Kumar, X. Wang, M. Kühnel, K. Nørgaard, R. C. Chiechi, *Nano Lett.* **2018**, *18*, 7552.
[10] G. Yang, S. Sangtarash, Z. Liu, X. Li, H. Sadeghi, Z. Tan, R. Li, J. Zheng, X. Dong, J. Liu, Y. Yang, J. Shi, Z. Xiao, G. Zhang, C. Lambert, W. Hong, D. Zhang, *Chem. Sci.* **2017**, *8*, 7505.
[11] C. Li, V. Stepanenko, M. J. Lin, W. Hong, F. Würthner, T. Wandlowski, *Phys. Status Solidi B* **2013**, *250*, 2458.
[12] C. Jia, M. Famili, M. Carlotti, Y. Liu, P. Wang, I. M. Grace, Z. Feng, Y. Wang, Z. Zhao, M. Ding, X. Xu, C. Wang, S. J. Lee, Y. Huang, R. C. Chiechi, C. J. Lambert, X. Duan, *Sci. Adv.* **2018**, *4*, eaat8237.
[13] Y. Li, M. Baghernejad, A. G. Qusiy, D. Zsolt Manrique, G. Zhang, J. Hamill, Y. Fu, P. Broekmann, W. Hong, T. Wandlowski, D. Zhang, C. Lambert, *Angew. Chem., Int. Ed.* **2015**, *54*, 13586.
[14] G. Ke, C. Duan, F. Huang, X. Guo, *InfoMat* **2020**, *2*, 92.
[15] A. C. Whalley, M. L. Steigerwald, X. Guo, C. Nuckolls, *J. Am. Chem. Soc.* **2007**, *129*, 12590.
[16] P. Chandra Mondal, U. M. Tefashe, R. L. McCreery, *J. Am. Chem. Soc.* **2018**, *140*, 7239.
[17] X. Qiu, R. C. Chiechi, *Trends Chem.* **2020**, *2*, P869.
[18] X. Qiu, V. Ivasyshyn, L. Qiu, M. Enache, J. Dong, S. Rousseva, G. Portale, M. Stöhr, J. C. Hummelen, R. C. Chiechi, *Nat. Mater.* **2020**, 330.
[19] J. A. Smerdon, N. C. Giebink, N. P. Guisinger, P. Darancet, J. R. Guest, *Nano Lett.* **2016**, *16*, 2603.
[20] Z. Xie, I. Bâldea, C. D. Frisbie, *Chem. Sci.* **2018**, *9*, 4456.
[21] S. J. Cho, G. D. Kong, S. Park, J. Park, S. E. Byeon, T. Kim, H. J. Yoon, *Nano Lett.* **2019**, *19*, 545.
[22] O. E. C. Ocampo, P. Gordiichuk, S. Catarci, D. A. Gautier, A. Herrmann, R. C. Chiechi, *J. Am. Chem. Soc.* **2015**, *137*, 8419.
[23] P. Gordiichuk, D. Pesce, O. E. Ocampo, A. Marcozzi, G. J. A. Wetzelaer, A. Paul, M. Loznik, E. Gloukhikh, S. Richter, R. C. Chiechi, A. Herrmann, *Adv. Sci.* **2017**, *4*, 1600393.
[24] C. A. Nijhuis, W. F. Reus, J. R. Barber, M. D. Dickey, G. M. Whitesides, *Nano Lett.* **2010**, *10*, 3611.
[25] L. Yuan, N. Nerngchamnong, L. Cao, H. Hamoudi, E. del Barco, M. Roemer, R. K. Sriramula, D. Thompson, C. A. Nijhuis, *Nat. Commun.* **2015**, *6*, 6324.
[26] L. Luo, L. Balhorn, B. Vlaisavljevich, D. Ma, L. Gagliardi, C. D. Frisbie, *J. Phys. Chem. C* **2014**, *118*, 26485.
[27] L. Qiu, Y. Zhang, T. L. Krijger, X. Qiu, P. v. t. Hof, J. C. Hummelen, R. C. Chiechi, *Chem. Sci.* **2017**, *8*, 2365.
[28] Y. Han, C. A. Nijhuis, *Chem. - Asian J.* **2020**, *151*, 3752.
[29] J. Chen, S. Gathiaka, Z. Wang, M. Thuo, *J. Phys. Chem. C* **2017**, *121*, 23931.
[30] J. Chen, M. Kim, S. Gathiaka, S. J. Cho, S. Kundu, H. J. Yoon, M. M. Thuo, *J. Phys. Chem. Lett.* **2018**, *9*, 5078.
[31] A. Alaghi, J. P. Hayes, *ACM Trans. Embed. Comput. Soc.* **2013**, *12*, 1.
[32] W. Qian, X. Li, M. D. Riedel, K. Bazargan, D. J. Lilja, *IEEE Trans. Comput.* **2011**, *60*, 93.
[33] C. M. Woodbridge, D. L. Pugmire, R. C. Johnson, N. M. Boag, M. A. Langell, *J. Phys. Chem. B* **2000**, *104*, 3085.
[34] R. C. Chiechi, E. A. Weiss, M. D. Dickey, G. M. Whitesides, *Angew. Chem., Int. Ed.* **2008**, *47*, 142.
[35] J. Trasobares, D. Vuillaume, D. Théron, N. Clément, *Nat. Commun.* **2016**, *7*, 1.
[36] F. C. Simeone, H. J. Yoon, M. M. Thuo, J. R. Barber, B. Smith, G. M. Whitesides, *J. Am. Chem. Soc.* **2013**, *135*, 18131.
[37] M. Baghbanzadeh, C. M. Bowers, D. Rappoport, T. Żaba, L. Yuan, K. Kang, K.-C. Liao, M. Gonidec, P. Rothemund, P. Cyganik, A. Aspuru-Guzik, G. M. Whitesides, *J. Am. Chem. Soc.* **2017**, *139*, 7624.
[38] S. Züfle, S. Altazin, A. Hofmann, L. Jäger, M. T. Neukom, W. Brütting, B. Ruhstaller, *J. Appl. Phys.* **2017**, *122*, 11.
[39] S. Kumar, M. Merelli, W. Danowski, P. Rudolf, B. L. Feringa, R. C. Chiechi, *Adv. Mater.* **2019**, *1*, 1807831.
[40] C. E. Shannon, *The Mathematical Theory of Communication*, The University of Illinois Press, Champaign, IL, USA **1971**.
[41] S. Verdu, *IEEE Trans. Inf. Theory* **1998**, *44*, 2057.
[42] X. Qiu, O. C. Ocampo, H. W. de Vries, M. van Putten, M. Loznik, A. Herrmann, R. C. Chiechi, *ACS Appl. Mater. Interfaces* **2018**, *10*, 37625.
[43] E. Douvogianni, X. Qiu, L. Qiu, F. Jahani, F. B. Kooistra, J. C. Hummelen, R. C. Chiechi, *Chem. Mater.* **2018**, *30*, 5527.